Quad-Modal Fluorescent Nanothermometers Based On Core/Shell $CuInS_2$/ZnS Quantum Dots

M. Duda[1], P. Joshi[1], A. Borodziuk[1], K. Sobczak[2], B. Sikora-Dobrowolska[1], S. Maćkowski[3], A .M. Dennis[4], Ł. Kłopotowski[1]*

[1] Institute of Physics, Polish Academy of Sciences, Warsaw, Poland
[2] University of Warsaw Biological and Chemical Research Centre, Warsaw, Poland
[3] Faculty of Physics, Astronomy and Informatics, Nicolaus Copernicus University, Toruń, Poland
[4] Department of Chemical Engineering, Northeastern University, Boston, United States

Introduction

Temperature detection is one of the key issues in intracellular research. Monitoring changes in the temperature allows us to track processes taking place in the cell. Therefore, it is important to find a non-invasive, non-toxic material that will enable temperature detection in individual parts of the cell. Colloidal CIS/ZnS QDs are the focus of interest due to their size-dependent luminescence, broadband absorption, low excitation energy, and lack of heavy metal ions. These properties enable the application of QDs in biological research as nanothermometers and make them a competitive material compared to other systems, e.g., fluorescent polymers, proteins, and upconverting nanoparticles. In our work, we aim to improve the sensitivity of the thermometer, to enable the most accurate temperature measurements.

Conclusions

- Our thermometer's readout modes are based on (i) PL intensity, (ii) PL lifetime, (iii) PL peak shift, and (iv) a PL intensity ratio under two specific excitation wavelengths which allowed us to obtain quad-modal fluorescent nanothermometer.
- All modes of our nanothermometer can be readily employed using confocal microscopes.
- The highest obtained sensitivity for our nanothermometer is based on the PL intensity mode and is equal to 3.2% - this value is the highest sensitivity among inorganic semiconductor QDs.
- The new MLR analysis method allowed us to obtain multiparametric temperature readout, which increased our thermometer's sensitivity up to 34%.
- Negligible changes in CIS/ZnS-30 absorbance, indicate that QDs are stable in an aqueous environment for 56 days.
- Temperature-induced changes in PL intensity and PL peak position are reproducible and reversible within 20-60°C temperature range.
- Confocal fluorescent microscope images of HeLa cells incubated with CIS QDs revealed that QDs successfully entered the HeLa cells.

CIS/ZnS QDs Optical properties

- Increased ZnS synthesis time blue-shifts PL and absorption spectra.
- Blue-shift → interplay of:(i) Zn for Cu cation exchange, (ii) etching of CIS QDs core, and (iii) formation of a ZnS shell.
- PL quantum yield enhanced over 10 times.

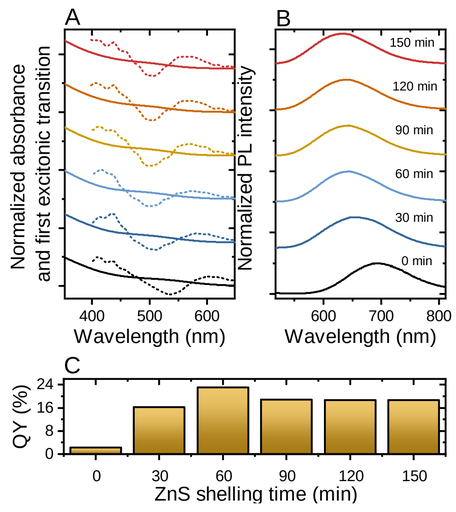

Fig. 1: A: Absorption and second derivative, and B: PL spectra of CIS/ZnS QDs after different ZnS synthesis times. C: Quantum yield of CIS/ZnS QDs with different ZnS synthesis times. The CIS and CIS/ZnS QDs were synthesized as described in Refs. [1, 2].

Quad-modal temperature readout

- As the temperature increases the PL intensity and the PL lifetime decrease due to thermal activation of non-radiative recombination.
- With increased temperature the PL position red-shifts, which is attributed to the closing of the bandgap
- PL intensity ratio under two specific excitation wavelengths depends on the temperature due to different activation energies for non-radiative recombination surface trapping

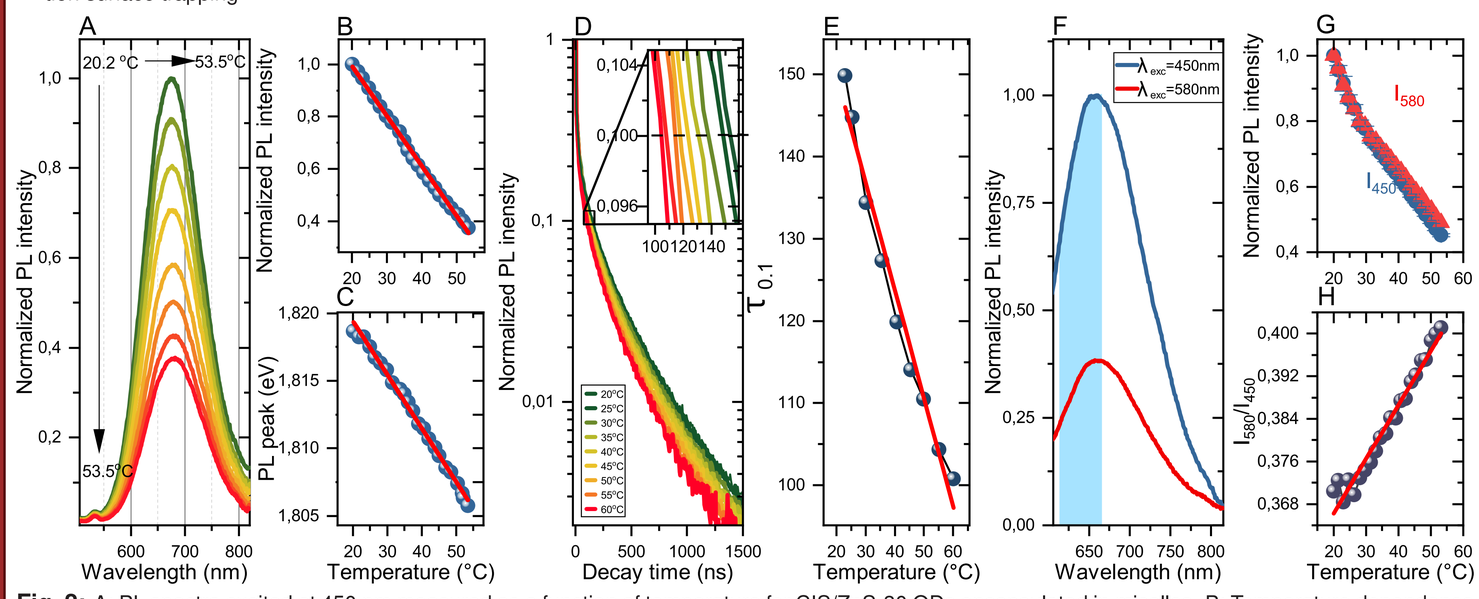

Fig. 2: A: PL spectra excited at 450 nm measured as a function of temperature for CIS/ZnS-30 QDs encapsulated in micelles. B: Temperature dependence of the normalized PL intensity (points). C: PL peak position as a function of temperature (points). D: Temperature dependence of normalized PL decays excited at 400 nm. E: Temperature dependence of PL lifetime ($\tau_{0.1}$). $\tau_{0.1}$ is defined as the decay time at which the intensity drops by a factor of 10. F: PL spectra after 450 (blue line) and 580 nm (red line) excitation. The blue area denotes the spectrum integration range. G: Normalized integrated PL intensities as a function of temperature, for excitation at 450 nm (I_{450}, blue circles) and 580 nm (I_{580}, red triangles). H: Temperature dependence of I_{450}/I_{580} ratio (blue points). Red lines represent linear fits to the data.

PL temperature-dependent processes

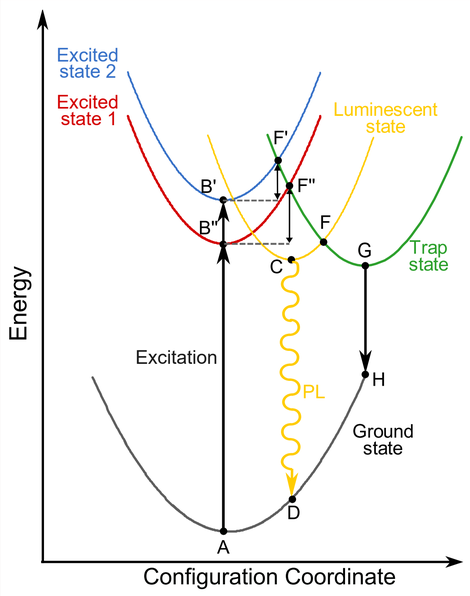

Fig. 3: Configuration coordinate diagram depicting the excitation, trapping, and recombination processes responsible for temperature-dependent PL processes. Solid upward and downward arrows denote, respectively, excitation and non-radiative recombination. The wavy arrow denotes radiative recombination. Double-headed arrows show the barrier heights for hot carrier trapping.

Multiparametric temperature sensing

We evaluated multiparametric sensitivity for our nanothermometers based on Ref. [4]. In the Multiple Linear Regression (MLR) method, the thermometric parameters (Q_i) have to vary linearly, so the temperature (T) can be expressed as $T = \beta_0 + \beta_1 Q_1 + ... + \beta_4 Q_4$, where the β_0 is the intercept and β_i is the slope of each Q_i. Then, the multiparametric sensitivity can be defined as: $S_{MLR} = \sqrt{\sum_{i=1}^{4}(Q_i\beta_i)^{-2}}$.

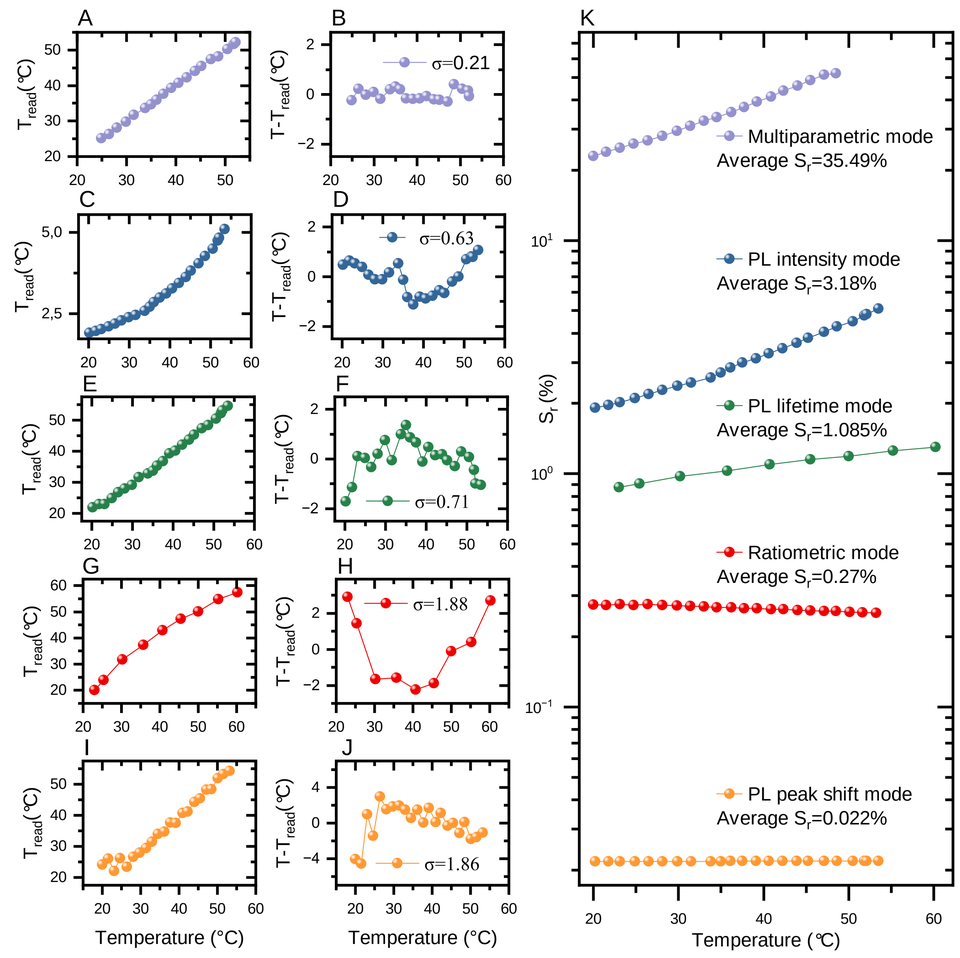

Fig. 4: A, C, E, G, I: Readout temperatures vs. the experimental temperatures. B, D, F, H, J: Temperature readout residuals indicating the precision of each mode (given in the legends). K: Sensitivities of the four readout modes and the multiparametric readout based on MLR.

Micelles encapsulation

- PL spectra of CIS/ZnS QDs encapsulated in micelles are slightly red-shifted
- Red-shift occurs as a result of changing the CIS/ZnS QDs environment to more polar.

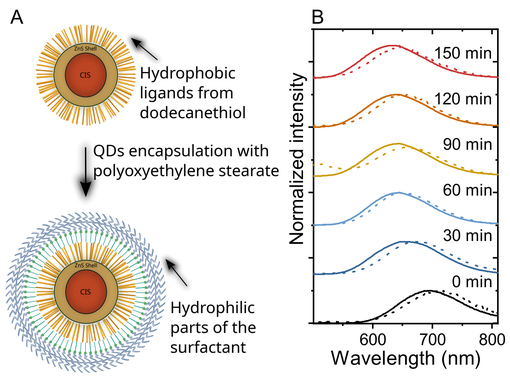

Fig. 5: A: Scheme of the micelles encapsulation. B: PL spectra for CIS/ZnS QDs dispersed in toluene (solid lines) and CIS/ZnS QDs encapsulated in micelles dispersed in water (dashed lines) with ZnS synthesis times. CIS/ZnS QDs encapsulated in micelles were prepared according to Ref. [3].

Nanothermometer's sensitivity

To compare the nanothermometer's performance, for each sample and readout mode the relative sensitivity was calculated based on the equation: $S_\xi = \left|\frac{1}{Q_\xi}\frac{dQ_\xi}{dT}\right|$, where ξ is I as intensity, E as PL maximum, τ as PL lifetime, or R as ratiometric mode.

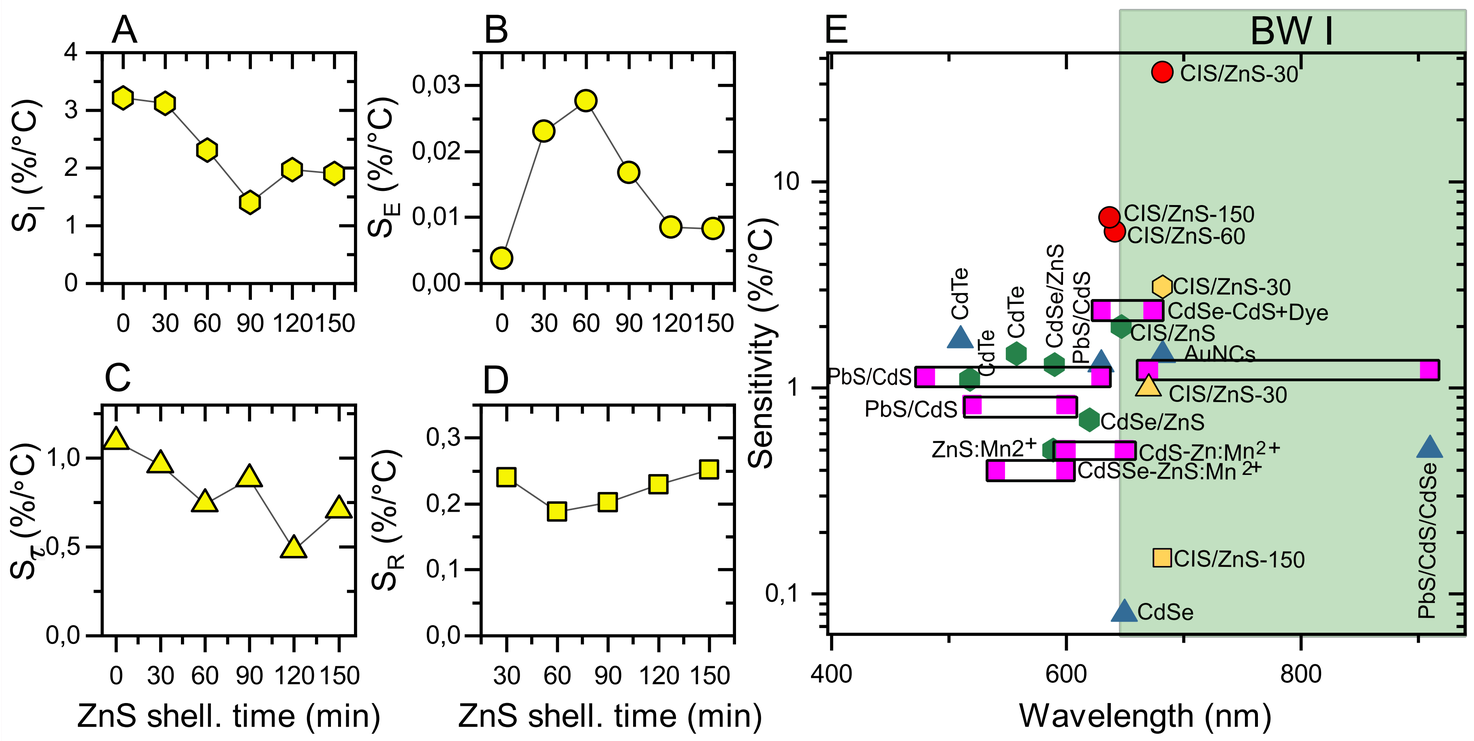

Fig. 6: Thermal sensitivities of the four readout modes based on A: PL intensity, B: PL peak shift C: PL lifetime, and D: PL intensity ratio after excitation at two wavelengths. E: Comparison of sensitivities plotted as a function of emission wavelength for different QD systems. The triangles, hexagons, and squares denote the sensitivity values for QD nanothermometers based on PL lifetime, PL intensity, and ratiometric mode, respectively. Yellow symbols represent the highest sensitivity values obtained for the QDs studied in our work. The red points represent the sensitivities of the multiparametric readout mode of our QDs. The green area marks the first biological window (BW I).

Stability and repeatability

- QDs structure remains intact over 56 days.
- Temperature-induced PL changes are reproducible and reversible.

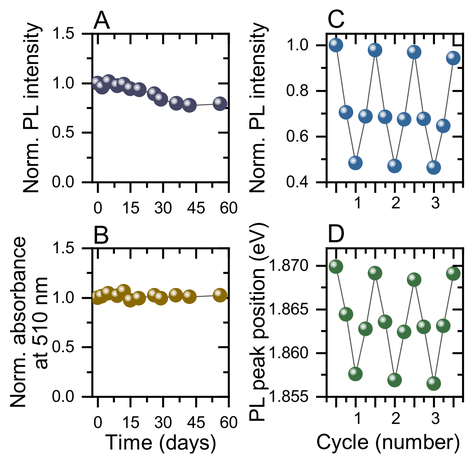

Fig. 7: Time dependence of A: PL intensity (λ_{exc}=450 nm) and B: normalized absorbance. C: PL intensity and D: PL peak position over 3 heating/cooling cycles (temp. range 20-60°C).

CIS/ZnS micelles in HeLa cells

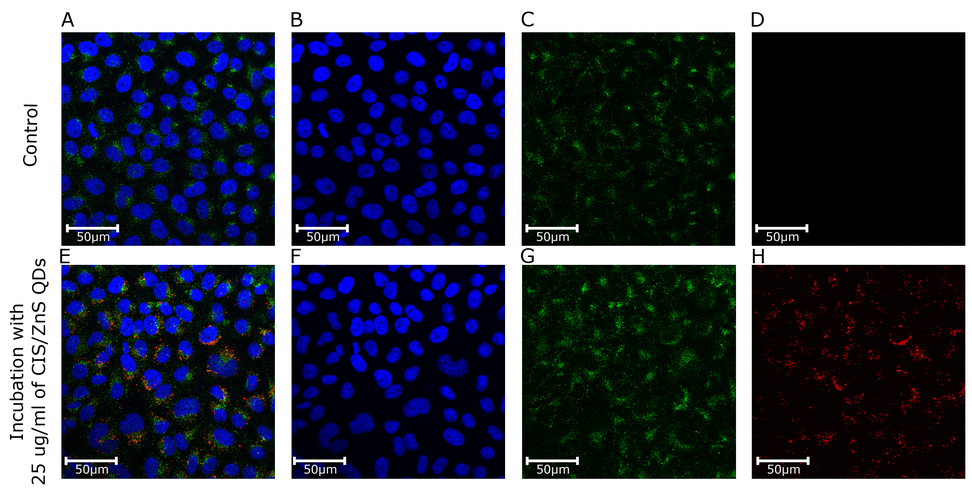

Fig. 8: The confocal microscope images of A-D: HeLa cells and E-G: HeLa cells incubated with 25μg of CIS/ZnS-120 QDs. A, E: Overlay image of blue, green, and red channels. B: and F: Images of cells with nuclei stained with Hoechst 33342 dye (blue channel, emission range 425-475 nm). C: and G: Images of cells with lysosomes stained with Alexa Fluor 488-conjugated protein (green channel, emission range 494-525 nm). D: and H: CIS/ZnS-120 QDs (red channel, emission range 590-740 nm). All scale bars correspond to 50 μm.

References

[1] Li L., et al., J. Am. Chem. Soc. 2011, 133, 5, 1176–1179
[2] Speranskaya E. S., et al., Langmuir, 2014, 30, 25, 7567– 7575
[3] Zhang H., et al., Mater. Chem. B, 2019,7, 2835-2844
[4] Maturi F. E., et al., Laser & Photonics Reviews, 2021, 15(11), 2100301

Contact

lklopot@ifpan.edu.pl*
mduda@ifpan.edu.pl

Acknowlegments

This work was supported by National Science Centre Poland grant no. 2019/35/B/ST3/04235 and the Project no. 2018/31/G/ST3/03596.